International Journal of Mechanical Sciences 82 (2014) 32–40

Contents lists available at ScienceDirect

International Journal of Mechanical Sciences

journal homepage: www.elsevier.com/locate/ijmecsci

Beneficial performance of a quasi-zero-stiffness vibration isolator with time-delayed active control

Xiuting Sun [a,b,*], Jian Xu [a], Xingjian Jing [b], Li Cheng [b]

[a] School of Aerospace Engineering and Applied Mechanics, Tongji University, Shanghai, PR China
[b] Department of Mechanical Engineering, The Hong Kong Polytechnic University, Hong Kong, PR China

ARTICLE INFO

Article history:
Received 6 March 2013
Accepted 3 March 2014
Available online 7 March 2014

Keywords:
Vibration isolator
Quasi-zero-stiffness
Time delay
Stability
Bifurcation

ABSTRACT

The potential beneficial performance of a quasi-zero-stiffness vibration isolator (QZS-VI) with a simple linear time-delayed active control strategy is investigated in this study. Stability and bifurcation analysis shows that an active control can basically improve the system robustness in stability at the equilibrium position. However, a time-delayed active control can not only further strengthen the robustness of the system in stability, but also noticeably improve system transmissibility performance both in force and base excitations and obviously decrease the settling time of system transient response subject to an impact load. Moreover, it is shown that the controlled stiffness and especially the introduced time delay could be designed deliberately so that undesirable bifurcation and chaotic behaviors can be avoided or greatly suppressed. The results provide a useful insight into the analysis and design of nonlinear vibration isolators by exploiting potential nonlinear benefits of the time delay in vibration control.

1. Introduction

Many damages of structures, such as fatigue and failure induced by vibration, often happen at a low excitation frequency in practical engineering [1]. Isolators are therefore widely used to suppress vibrations in order to lengthen the service life of equipments and structures and to provide a more comfortable and safe condition for human beings. When the frequency of external harmonic excitation is $\omega > \sqrt{2}\omega_0$, where ω_0 is the natural frequency of the system, the isolator can usually provide efficient vibration suppression [2]. The most common method of isolating vibrations at low frequency is to use an isolator whose stiffness is close to zero [3–7]. This kind of isolators are referred to as quasi-zero-stiffness vibration isolators (QZS-VIs), which in structure are often connected to the base by two horizontal springs and a vertical spring. QZS-VI system has many advantages such as small static displacement, small dynamic stiffness and low natural frequency. In [3–9], the QZS-VI system is demonstrated to be an ultra-low frequency vibration isolator by adjusting the stiffness characteristics and geometric size of the two horizontal springs. It is shown that the system can offer excellent performance in vibration isolation under force and base excitations at low frequency from theoretical analysis and experiment results [7]. Although the advantages of the QZS-VI system are well recognized in the mentioned results, the resonance peak of the system is often considerably large and the inherent nonlinearity could induce jump phenomenon at around the resonant frequency, which may not be expected in practice due to safety and stability.

Therefore, it is important to improve the system to obtain much better isolation performance. The dynamical equation of a QZS-VI can be described by a single-DOF oscillator with cubic nonlinearity [10–14], and the latter could also be used to describe the dynamics of a vibration absorber. Although few works have been done directly for the active control of QZS-VI, many studies have been conducted for the Duffing oscillator and vibration absorbers [15–18]. It is noticed that, to suppress the vibration at around the resonant frequency, time-delayed active control strategies have been investigated for vibration absorbers and significant vibration suppression performance is thus achieved [15,16]. Nana et al. [17,18] design a control device focusing on single or double Duffing oscillators with time-delayed control strength. The previous results indicate clearly that the parameters of the control law to be designed including the time delay and magnitude etc. actually play a crucial role in the effectiveness of the active control. However, systematical investigation on the nonlinear effect incurred by the time delay to the QZS-VI system is still yet to be developed. In order to study the complex nonlinear behaviors induced by time delay in dynamical systems [19], dynamic performance of a QZS-VI system subject to a time-delayed active

* Corresponding author at: School of Aerospace Engineering and Applied Mechanics, Tongji University, Shanghai, PR China.
E-mail address: 05mech_sunxiuting@tongji.edu.cn (X. Sun).

http://dx.doi.org/10.1016/j.ijmecsci.2014.03.002
0020-7403

control is investigated in this study. The potential beneficial vibration isolation performance incurred by the specially-introduced time delay under different loading/excitation conditions is systematically studied with both theoretical analysis and simulation studies. It is shown that the controlled stiffness and especially the introduced time delay could be designed properly so that system transmissibility performance both in force and base excitations and system impact response subject to an impact load can all be much improved, and undesirable bifurcation and chaotic behaviors can also be avoided or greatly suppressed.

The paper is organized as follows. Firstly, a QZS isolator with active control is introduced and modeled in Section 2. The stability and bifurcation analysis is conducted for the system to show the range of physical parameters to guarantee stability. Secondly, the nonlinear effect of a time-delayed active control is systematically analyzed for the QZS-VI system considering three different cases in impact load, force and displacement excitations in Section 3. Both force transmissibility and displacement transmissibility are studied and bifurcation behaviors incurred by the time delay are discussed with Harmonic balance methods [20,21]. A conclusion is thereafter given in Section 4.

2. The QZS vibration isolator (QZS-VI)

2.1. The isolator

The schematic structure of the QZS-VI with an active control device is shown in Fig. 1 [7]. The mass is the equipment to be isolated from the Base, which is connected to the base through (a) two horizontal springs with a linear stiffness k_1 and nonlinear stiffness k_2 with the connecting bar of the length a, (b) a vertical spring with stiffness k_0 and (c) an active control device. The one end of the horizontal spring is fixed to the Base and the other end is connected to a roller, which is free to slide in horizontal direction. The roller is linked to the connecting bar, while the latter is jointed to the mass. Therefore, the mass can move in the vertical direction. The active control device is fixed on the base including a vertical spring with stiffness k_3 and a servo motor which provides an active feedback force to the vertical spring. Therefore, the vertical spring is also referred to as controlled spring. The nomenclature is shown in Table 1.

2.2. Modeling

Fig. 2 is the free-body diagram for a connecting element. The relationship between the restoring force F and the displacement y can be found by the principal of virtual work.

The geometrical relationship of the virtual displacement in two direction δx and δy is $\delta x = y\,\delta y/\sqrt{a^2-y^2}$. Therefore, the relationship between the restoring force F and the displacement y can be derived. The total work done by the restoring force F, the horizontal restoring force F_2, the restoring force of vertical spring F_1 and control spring F_3, should be zero, i.e.

$$F\,\delta y - F_1\,\delta y - F_3\,\delta y + 2F_2\frac{y}{\sqrt{a^2-y^2}}\delta y = 0 \tag{1}$$

The restoring force can then be given as

$$F(y) = (k_0+k_3)y - 2\left\{k_1[\lambda_0-(a-\sqrt{a^2-y^2})]+k_2[\lambda_0-(a-\sqrt{a^2-y^2})]^3\right\}\frac{y}{\sqrt{a^2-y^2}} \tag{2}$$

Introducing the dimensionless parameters

$$\hat{F}(y)=\frac{F(y)}{ak_0},\quad \hat{y}=\frac{y}{a},\quad \hat{\lambda}=\frac{\lambda_0}{a},\quad \alpha_1=\frac{k_1}{k_0},\quad \alpha_2=\frac{k_2}{k_0},\quad g=\frac{k_3}{k_0}. \tag{3}$$

The expression of dimensionless restoring force is

$$\hat{F}(\hat{y}) = (1+g)\hat{y} - 2\left\{\alpha_1[\hat{\lambda}-(1-\sqrt{1-\hat{y}^2})]+a^2\alpha_2[\hat{\lambda}-(1-\sqrt{1-\hat{y}^2})]^3\right\}\frac{\hat{y}}{\sqrt{1-\hat{y}^2}} \tag{4}$$

Table 1
The physical parameters of the isolator

Physical parameters	Symbol	Unit
Compression deformation	λ_0	[m]
Length of the connecting element	a	[m]
Linear stiffness of horizontal springs	k_1	[N m^{-1}]
Nonlinear stiffness of horizontal springs	k_2	[N m^{-3}]
Stiffness of vertical spring	k_0	[N m^{-1}]
Stiffness of control spring	k_3	[N m^{-1}]
Origin length of horizontal springs	l_0	[m]
Displacement of Base excitation	z_e	[m]

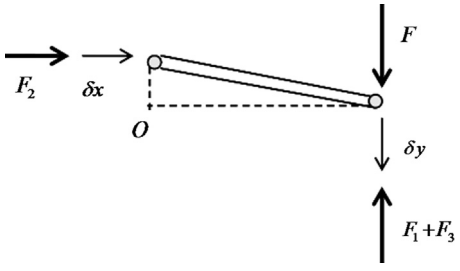

Fig. 2. The principle of virtual work.

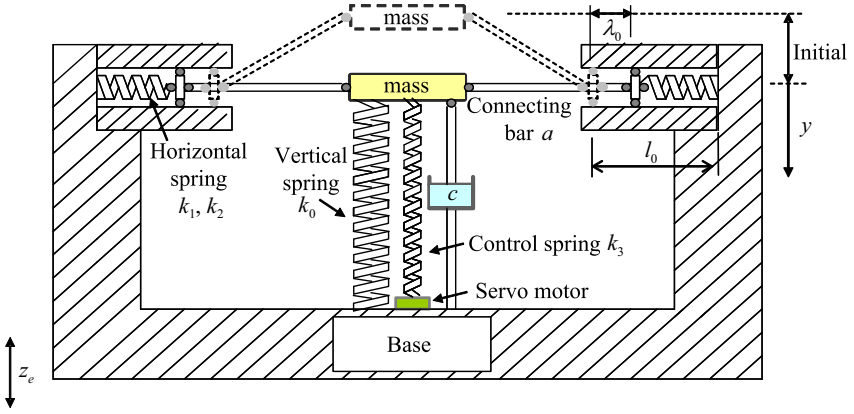

Fig. 1. Scheme of quasi-zero-stiffness vibration isolator device.

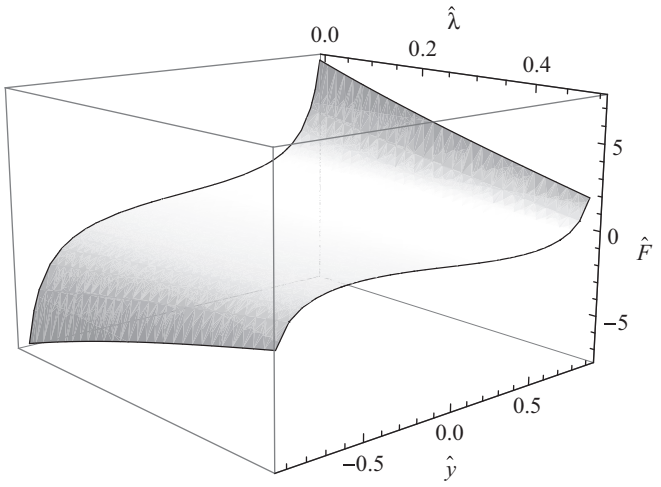

Fig. 3. The influence of the pre-compression parameters $\hat{\lambda}$ on the restoring force for $\alpha_1=2$, $\alpha_2=5$, and $a=0.4$.

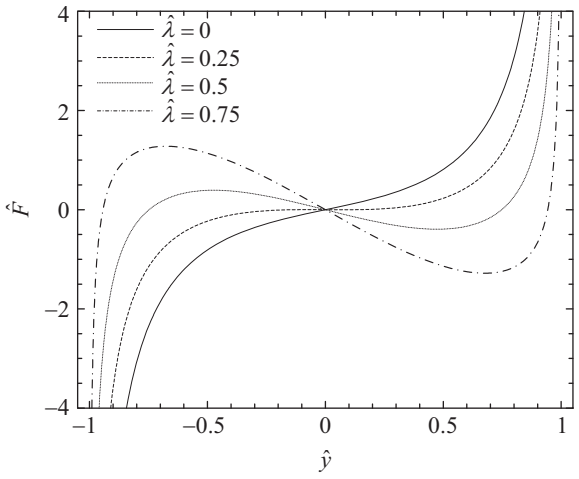

Fig. 4. The dimensionless restoring force-displacement characteristic under different pre-compression for $\alpha_1=2$, $\alpha_2=5$, and $a=0.4$.

The equation above indicates that the stiffness of the system is affected by the geometry parameter a, the pre-compression parameter $\hat{\lambda}$ and the stiffness parameters k_0, k_1, k_2 and k_3. By adjusting these parameters, the linear stiffness of the QZS-VI can be changed from positive to negative. As a result, the resonant frequency of the QZS-VI can be reduced to a low level.

Fig. 3 shows the relation between the nonlinear force and the parameters for $\alpha_1=2$, $\alpha_2=5$, and $a=0.4$. It is seen from Fig. 3 that the linear stiffness of the QZS-VI is changed from positive to negative as $\hat{\lambda}$ increases. Fig. 4 is the relationship between the restoring force $\hat{F}$ and the displacement under different pre-compression for some values of $\hat{\lambda}$. It follows from Fig. 4 that the gradient of the restoring force changes profoundly depending on the value of the pre-compression $\hat{\lambda}$. The QZS-VI has displacement ranges with negative stiffness when the value of pre-compression increases.

2.3. Stability and bifurcation analysis

Form the analysis above, it is found that the linear part of the QZS-VI decreases with the pre-compression increasing. However, if the coefficients of the restoring force are improperly changed, the equilibrium position of the QZS-VI is unstable, which can induce danger in practice. Thus, to maintain the stability of equilibrium position, the pre-compression $\hat{\lambda}$ and other parameters of the system are required to stay in a reasonable range. The stability of the equilibrium position is analyzed from the dynamical equation of the system. The equation of the system can be written as follows:

$$M\ddot{y}+c\dot{y}+F(y)=f(t) \tag{5}$$

The dimensionless parameters are chosen as

$$\hat{y}=\frac{y}{a},\quad \hat{\lambda}=\frac{\lambda_0}{a},\quad \omega_0^2=\sqrt{\frac{k_0}{M}},\quad t'=\omega_0 t,\quad \hat{F}(\hat{y})=\frac{F(y)}{ak_0},$$
$$\alpha_1=\frac{k_1}{k_0},\quad \alpha_2=\frac{k_2}{k_0},\quad g=\frac{k_3}{k_0},\quad \xi=\frac{c}{2\sqrt{Mk_0}},\quad \hat{f}(t)=\frac{f(t)}{ak_0}. \tag{6}$$

The dimensionless dynamical equation is then given by

$$\ddot{\hat{y}}+2\xi\dot{\hat{y}}+\hat{F}(\hat{y})=\hat{f}(t') \tag{7}$$

where $\hat{F}(\hat{y})$ is the dimensionless force as shown in Eq. (4). The stability of the equilibrium position of Eq. (7) should be studied to reveal the range of the adjustable structural parameters of the system. Note that the dimensionless force $\hat{F}(\hat{y})$ is a nonlinear function. The Taylor series expansion is employed for an approximation. $\hat{F}(\hat{y})$ in Eq. (7) can then be expanded with the Taylor series up to the third or fifth order as follows:

$$\hat{F}(\hat{y})=\beta\hat{y}+g\hat{y}+\gamma_1\hat{y}^3 \tag{8}$$

or

$$\hat{F}(\hat{y})=\beta\hat{y}+g\hat{y}+\gamma_1\hat{y}^3+\gamma_2\hat{y}^5 \tag{9}$$

where

$$\beta=1-2\alpha_1\hat{\lambda}-2a^2\alpha_2\hat{\lambda}^3,\gamma_1=\alpha_1(1-\hat{\lambda})+a^2\alpha_2(3\hat{\lambda}^2-\hat{\lambda}^3),$$
$$\gamma_2=\frac{3}{4}[\alpha_1(1-\hat{\lambda})+a^2\alpha_2(3\hat{\lambda}^2-2\hat{\lambda}-\hat{\lambda}^3)]. \tag{10}$$

Fig. 5 shows the accuracy of the third order and fifth order Taylor series expansion in fitting the restoring force. It can be seen

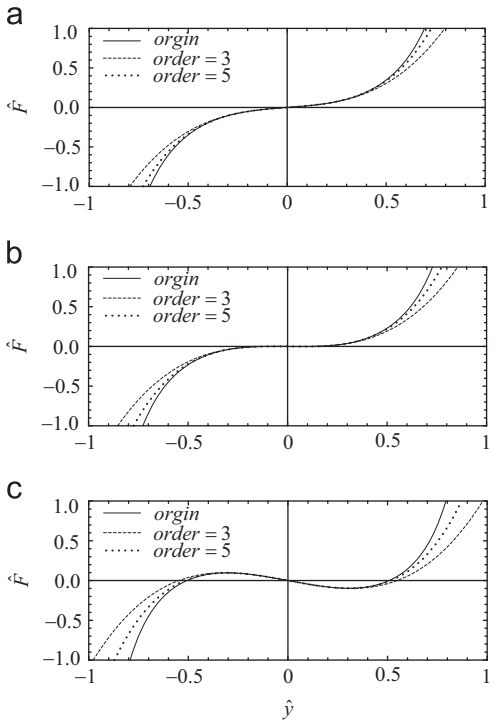

Fig. 5. Third order and fifth order Taylor expansion fitting the restoring force curve under different pre-compression. (a) $\hat{\lambda}=0.15$, (b) $\hat{\lambda}=0.25$, (c) $\hat{\lambda}=0.35$ for $\alpha_1=2$, $\alpha_2=5$, and $a=0.4$.

from Fig. 5 that the difference between the fifth order Taylor expansion and the restoring force in Eq. (4) is quite small. Therefore, in the following analysis, the fifth Taylor series expansion is used to represent the dimensionless force in Eq. (7).

2.3.1. Pure passive control

The stability of the QZS-VI without the active control device is studied firstly. Thus, there is the condition that the coefficient $g=0$ in Eq. (9). The stability of the equilibrium depends on the eigenvalues of the system [10–12]. Ignoring the damping term in Eq. (7), the dynamical equation of the system can be written as

$$\dot{\hat{y}} = g_1(\hat{y},\hat{x}) = \hat{x}$$
$$\dot{\hat{x}} = g_2(\hat{y},\hat{x}) = \hat{F}(\hat{y}) \tag{11}$$

where $\hat{F}(\hat{y})$ is fifth order Taylor expansion as Eq. (9). Letting $g_1(\hat{y},x)=0$ and $g_2(\hat{y},x)=0$, the five equilibrium points of the system are defined as P_0, $P_1^{\pm}$ and $P_2^{\pm}$ which can be obtained as

$$P_0=(0,0), P_1^{\pm}=(\hat{y}_1^{\pm},0), P_2^{\pm}=(\hat{y}_2^{\pm},0) \tag{12}$$

where $\hat{y}_1^{\pm}=\pm\sqrt{(\gamma_1-\sqrt{\gamma_1^2-4\beta\gamma_2})/2\gamma_2}$, $\hat{y}_2^{\pm}=\pm\sqrt{(\gamma_1+\sqrt{\gamma_1^2-4\beta\gamma_2})/2\gamma_2}$, and β, γ_1, $\gamma_2>0$ are given by Eq. (10). The existence of the equilibrium points can be determined by (12). It is a trivial equilibrium P_0 for $(\gamma_1\pm\sqrt{\gamma_1^2-4\beta\gamma_2})<0$, three equilibriums P_0 and $P_2^{\pm}$ for $\gamma_1-\sqrt{\gamma_1^2-4\beta\gamma_2}<0$ and $\gamma_1+\sqrt{\gamma_1^2-4\beta\gamma_2}>0$, and five equilibriums for $\gamma_1-\sqrt{\gamma_1^2-4\beta\gamma_2}>0$, namely, $P_2^{\pm}$ exists for $\beta<0$ or $\beta>0$ and $\gamma_1<0$. Similarly, $P_1^{\pm}$ exists for $\beta>0$ and $\gamma_1<-2\sqrt{\beta\gamma_2}$, as shown in Fig. 6, where the curves bounded by the equilibrium number are given by

$$B=\{(\hat{\lambda},\ a)|\beta=0 \text{ and } \gamma_1\geq 0\},$$
$$H=\{(\hat{\lambda},\ a)|\beta=0,\gamma_1<0\},$$
$$D=\{(\hat{\lambda},\ a)|\beta>0 \text{ and } \gamma_1=-2\sqrt{\beta\gamma_2}\},$$

and only P_0 exists in Region 1, P_0 and $P_2^{\pm}$ exist in Region 2, and P_0, $P_1^{\pm}$ and $P_2^{\pm}$ in region 3.

The stability of the equilibriums can be determined by the eigenvalues of Jacobian Matrix of (11) which can be given by

$$J_{(\hat{y},\hat{x})}=\begin{bmatrix}\frac{\partial g_1}{\partial \hat{y}} & \frac{\partial g_1}{\partial \hat{x}}\\ \frac{\partial g_2}{\partial \hat{y}} & \frac{\partial g_2}{\partial \hat{x}}\end{bmatrix}=\begin{bmatrix}0 & 1\\ \frac{\partial \hat{F}(\hat{y})}{\partial \hat{y}} & 0\end{bmatrix}=\begin{bmatrix}0 & 1\\ \beta+3\gamma_1\hat{y}^2+5\gamma_2\hat{y}^4 & 0\end{bmatrix} \tag{13}$$

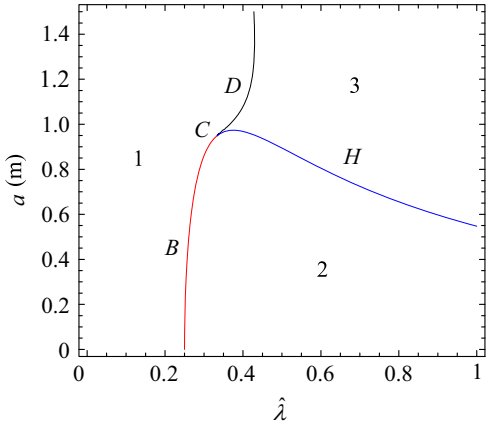

Fig. 6. Distribution of equilibriums in the parameter plane $(\hat{\lambda},a)$ for Eq. (11) when $\alpha_1=2$ and $\alpha_2=-5$.

If there are eigenvalues of Eq. (13) having negative real parts, the corresponding equilibrium is stable, otherwise unstable.

The parameters $(\hat{\lambda},a)$ take an important role in generating bifurcation behaviors of the system. To understand more, consider a potential function of the system as

$$V(\hat{y})=(1/2)\beta\hat{y}^2+(1/4)\gamma_1\hat{y}^4+(1/6)\gamma_2\hat{y}^6 \tag{14}$$

By fixing the parameters $(\hat{\lambda},a)$ in different regions in Fig. 6, different forms of potential function curve can be obtained, which shows the different number and stability type of equilibrium points.

Fig. 7 shows the potential function of the system when $(\hat{\lambda},a)$ are fixed in three different regions in Fig. 6. In region 1, the potential function $V(\hat{y})$ has one trap, which means P_0 is stable. The equilibrium position P_0 is unstable in region 2 and two additional traps corresponding to stable equilibrium $P_1^{\pm}$ appear. P_0 and two additional stable equilibrium points $P_2^{\pm}$ appear in region 3 while$P_1^{\pm}$ are unstable. These imply that the design of the pre-compression $\hat{\lambda}$ and the structural parameter a could avoid system dynamics trapped into regions 2 and 3 in order to ensure safety.

2.3.2. Active control using the controlled spring only

The active control device consists of a controlled spring and a servo motor. Under the static condition, the servo motor does not work, and the controlled spring can be fully used to strengthen the stability of the system as an ordinary spring. Therefore, considering only the influence of the controlled spring on the equilibrium position, the restoring force $\hat{F}(\hat{y})$ under the static condition becomes Eq. (9) and the coefficient $g\neq 0$. The parameter plane $(\hat{\lambda},a)$ is divided into three regions by the similar analysis in Section A.

In Fig. 8, the dashed lines are obtained by the study in Section A which satisfies $g=0$ while solid lines are obtained with the condition $g\neq 0$. From Fig. 8, it is found that the size of region 1 of the parameter plane $(\hat{\lambda},a)$ for $g\neq 0$ is larger than that for $g=0$, which indicates clearly that the controlled spring (although in a pure passive manner) helps the stability of the system.

Now, we explain the principle of the additional controlled spring in detail. In fact, t follows from Eqs. (7–10) that the addition controlled spring, namely g or k_3 shown in Fig. 1, increases the linear stiffness of the isolator. Thus, such controlled spring can efficiently modify the frequency of the isolator by just adding vertical stiffness so that the isolator can also enhance the system stability of the trivial equilibrium as shown in Fig. 8.

3. The QZS-VI system subject to a linear time-delayed active control

The isolation performance of the QZS-VI system under different load/excitation conditions are investigated to reveal the potential nonlinear effects incurred by the time delay in this section. The stiffness parameter g of the controlled spring and the time delay τ are focused. When the feedback states used by the servo motor is a time-delayed term $y(t-\tau_k)$, the dynamical equation of the isolator with this active control is modeled as

$$\ddot{\hat{y}}+2\xi\dot{\hat{y}}+\hat{F}(\hat{y})=g(\hat{y}_\tau-\hat{y})+\hat{f}(t') \tag{15}$$

where $\hat{F}(\hat{y})$ is given by Eq. (4) and the dimensionless time-delay $\tau=\omega_0\tau_k$ while τ_k is the real time-delay in the active control, $g(\hat{y}_\tau-\hat{y})=g(\hat{y}(t'-\tau)-\hat{y}(t'))$ is a control function [16] and g $(=k_3/k_0)$ is the additional stiffness as shown in Fig. 1. It is easy to see that the control function is absent for $\tau=0$ or without the delayed control. It has advantage to chose such control function. Firstly, such control function or delay control does not affect the

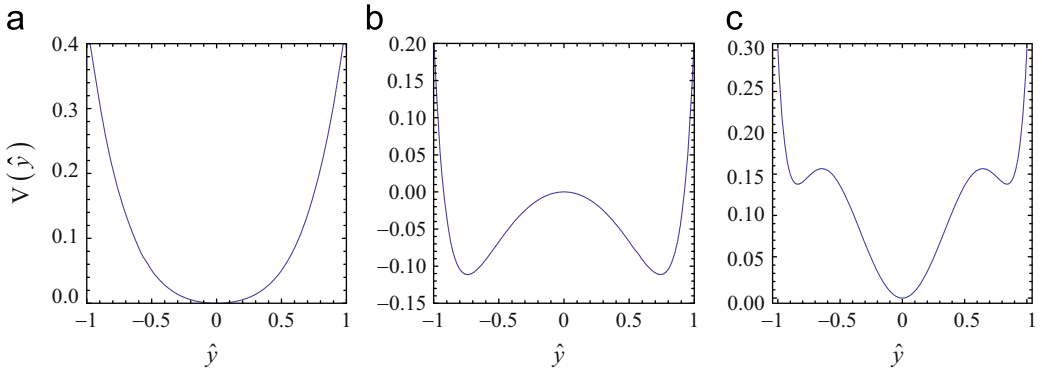

Fig. 7. The potential function of the system as parameters $(\hat{\lambda}, a)$ fixed in different regions. (a) $\hat{\lambda}=0.2$, $a=0.8$; (b) $\hat{\lambda}=0.5$, $a=0.6$; (c) $\hat{\lambda}=0.6$, $a=1.2$.

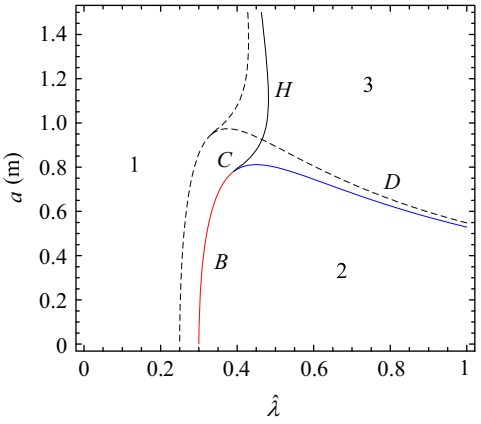

Fig. 8. The division on parameter plane of equilibrium point for considering the control spring.

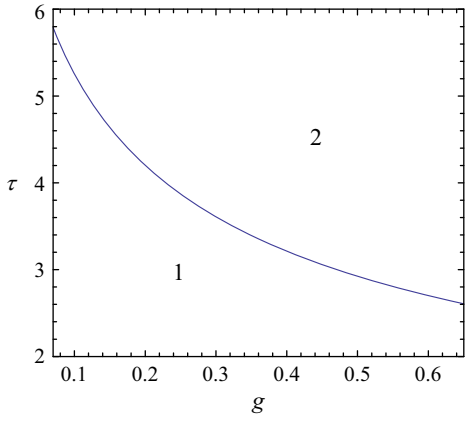

Fig. 9. The critical Hopf-bifurcation curve in parameter plane (g, τ).

position of the existed equilibria but does affect the stability and dynamic response of the system. Thus, it is possible to realize the dynamic control. Secondly, one is easy to compare those results from both uncontrolled and controlled isolators. Thirdly, the delay can be considered as a "switch" or an active quantity to achieve the required goal. This can be studied through the eigenvalues of the system with the time delay. The characteristic equation of the linear part of Eq. (15) is

$$\lambda^2+2\xi\lambda+\beta=ge^{-\lambda\tau}-g \tag{16}$$

To investigate the nonlinear effect of the time delay, the eigenvalues can be solved by substituting $\lambda=\alpha+i\omega$ into Eq. (16), which can be used to reveal the motion characteristics of the system under different values of time delay. The real part of the eigenvalues reflects the stability of the motion while the imaginary parts show the mode. To have the same the steady-state response as that without time delay, the critical boundary of the time delay should be derived. Setting $\alpha=0$ and substituting $\lambda=i\omega$ into the Eq. (16), the following equation can be obtained

$$-\omega^2+2\xi i\omega+\beta=ge^{-i\omega\tau}-g \tag{17}$$

Separating the real and imaginary part of the equation above, it can be obtained that

$$\begin{aligned}-\omega^2+\beta&=g\ \cos\ \omega\tau-g\\ 2\xi\omega&=-g\ \sin\ \omega\tau\end{aligned} \tag{18}$$

The frequency ω and critical value of the time delay can be solved as

$$\begin{aligned}\omega&=\sqrt{(\beta+g)-2\xi^2+\sqrt{[(\beta+g)-2\xi^2]^2-(\beta^2+2\beta g)}}\\ \tau_c&=\tfrac{1}{\omega}\arccos\left(\tfrac{\omega^2-\beta-g}{g}\right)\end{aligned} \tag{19}$$

The critical Hopf-bifurcation curve on the parameter plane (τ, g) can then be obtained according to Eq. (19) shown in Fig. 9.

In region 1 of Fig. 9, the real parts of eigenvalues are negative and the motion of the system decays with time. On the curve shown in the parameter plane (g, τ) in Fig. 9, the eigenvalues have zero real parts and the system undergoes Hopf bifurcation. The real parts of the eigenvalues become positive as the parameters are fixed in region 2 and the isolator system is in periodic vibration induced by the Hopf-bifurcation which causes the unstable of the equilibrium of the system. The parameter g is the dimensionless stiffness of the controlled spring and it indicates the control strength of the active control. From Fig. 9, with the increase of the value of coefficient g, the critical value of the time-delay decreased. Therefore, the control strength g should be confined above a reasonable threshold value since too small value for g may induce the Hopf-bifurcation (stable periodic vibration and unstable equilibrium) of the system.

The results above indicate that the time delay could greatly affect system dynamic response characteristics such as the stability and vibration suppression performance. Complex dynamic behaviors (both undesirable and beneficial) could also be generated due to the introduced time delay coupled with the inherent nonlinearity. To reveal more clearly the nonlinear effects incurred by the time delay in the active control, the vibration performance

of the QZS-VI system under three different load/excitation cases will be investigated in the following.

3.1. Dynamic response characteristics subject to impact loads on the mass

The dynamical equation of the isolator system is Eq. (15) where the impact load $\hat{f}(t')$ is

$$\hat{f}(t')=\begin{cases}\sin t', & t'<1\\ 0, & t'>1\end{cases} \tag{20}$$

Simulation results indicate that the time in the dynamic response subject to the impact load above is reduced obviously by the time-delayed active control and the time delay is a key parameter to suppress the transient response due to impact loading. The system impact response could have the fastest decay speed when the real parts of system eigenvalues are at a proper value. To find the most efficient time delay in suppressing impact response, the real parts of the eigenvalues under different time delays are calculated and the maximum value of real parts are obtained and shown in Fig. 10. It can be seen that, with the increase of the time delay but below an optimal value (i.e., the bottom of the curve in Fig. 10), the maximum real part of eigenvalues decreases. Then as the time delay reaches the optimal value, the maximum real part of eigenvalues increases until it approaches the zero level. The optimal time delay for impact response suppression should the one which can make the system to have eigenvalues with the smallest real part (corresponding to the optimal value of the time delay).

Fig. 11 is the time-series response of the system under different values of time delay as $g=0.3$. It can be seen that the settling time is shortest for $\tau=1.5$, which is consistent with the analysis above which $\tau=1.5$ is the optimal value for the time delay in this case and the real part of eigenvalues decreases for τ from zero to 1.5. Importantly, the value of the time delay should be limited in the range $(0,\tau_c)$ to avoid instability due to Hopf-bifurcation as mentioned before. In Fig. 12, the time-series responses are although periodic, yet cannot be suppressed since the value of the time delay $\tau\geq\tau_c$ due to the Hopf-bifurcation induced.

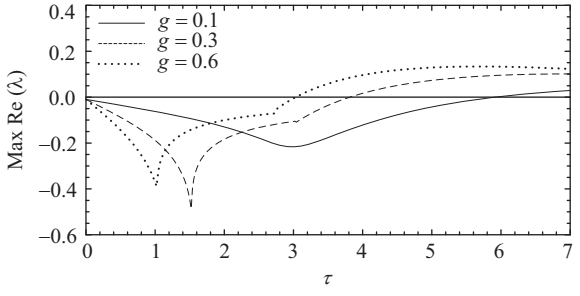

Fig. 10. The value of real part of eigenvalues of the system under different control coefficient g.

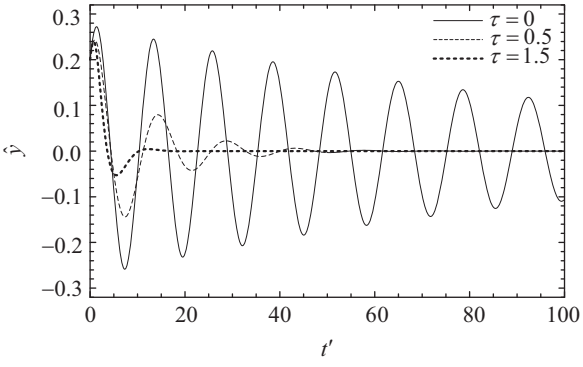

Fig. 11. The response of the system under the impact load with $g=0.3$, $\alpha_1=2$, $\alpha_2=5$, $a=0.4$ and $\hat{\lambda}=0.2$ under different time-delay.

3.2. Force transmissibility subject to force excitation on the mass

When the mass in Fig. 1 is under a harmonic excitation, the response amplitude of the system should be controlled as little as possible, which in practice is helpful for reducing noise and lengthening service life of structures and equipments etc. Considering the harmonic excitation $F=f\ \cos(\omega_e t+\theta)$ on the mass, the dimensionless dynamical equation is

$$\ddot{\hat{y}}+2\xi\dot{\hat{y}}+\hat{F}(\hat{y})=g(\hat{y}_\tau-\hat{y})+\hat{f}\ \cos(\Omega t'+\theta) \tag{21}$$

where the dimensionless amplitude of external excitation $\hat{f}=f/k_0$, the dimensionless frequency of the excitation $\Omega=\omega_e/\omega_0$.

Because of the damping term in the equation above, the free vibration term will decay and the response of the system is the particular solution caused by the external excitation. If the amplitude of the external excitation is too small to induce bifurcation, the response of the system is only periodic motion. Therefore, the harmonic balance method (HBM) can be employed to find the steady-state response of the system. The single-mode HBM solution can be written as

$$\hat{y}=A\ \cos(\Omega t') \tag{22}$$

Substituting the approximation periodic solution into Eq. (21), and separating the coefficients of the same harmonic components, the steady-state condition can be obtained as follows:

$$\begin{aligned}&Ag+A\beta+\frac{3}{4}A^3\gamma_1+\frac{5}{8}A^5\gamma_2-A\Omega^2-\hat{f}\ \cos\theta-Ag\ \cos(\Omega\tau)=0\\&-2A\xi\Omega+\hat{f}\ \sin\theta-Ag\ \sin(\Omega\tau)=0\end{aligned} \tag{23}$$

Therefore, the frequency-amplitude relationship under different time delay can be obtained as

$$\begin{aligned}&\left[A(g+\beta-\Omega^2-g\ \cos\Omega\tau)+\frac{3}{4}A^3\gamma_1+\frac{5}{8}A^5\gamma_2\right]^2\\&+(2A\xi\Omega+Ag\ \sin\Omega\tau)^2=\hat{f}^2\end{aligned} \tag{24}$$

The force transmissibility, defined by the ratio of the magnitude of the force transmitted to the base and the magnitude of the excitation force, i.e.,

$$|T_f|=\frac{\hat{f}_t}{\hat{f}} \tag{25}$$

is given by

$$|T_f|=\sqrt{\frac{\left[A(g+\beta-g\ \cos\Omega\tau)+(3/4)A^3\gamma_1+(5/8)A^5\gamma_2\right]^2+(2A\xi\Omega+Ag\ \sin\Omega\tau)^2}{\hat{f}^2}} \tag{26}$$

By fixing $(\hat{\lambda},a)$ in region 1 of Fig. 6 with $\hat{\lambda}=0.2$, $a=0.4$ and $g=0.5$, the force transmissibility under different values of the time delay is shown in Fig. 13.

For the external harmonic excitation, it follows from Fig. 13 that a jump behavior and large amplitude appear in the resonant region without the delayed control for $\tau=0$ and the response amplitude is quickly suppressed with the delay increasing, namely $\tau=0.2$, $\tau=0.4$ and $\tau=0.6$. It suggests that the time delay has significant effect on vibration suppression in this region. However, the transmissibility of control system is slightly greater than that of the passive system at the isolation region. It is concluded that one does not switch the delayed control for the effective frequencies of the isolator but switch the delayed or active control when the isolator is invalid.

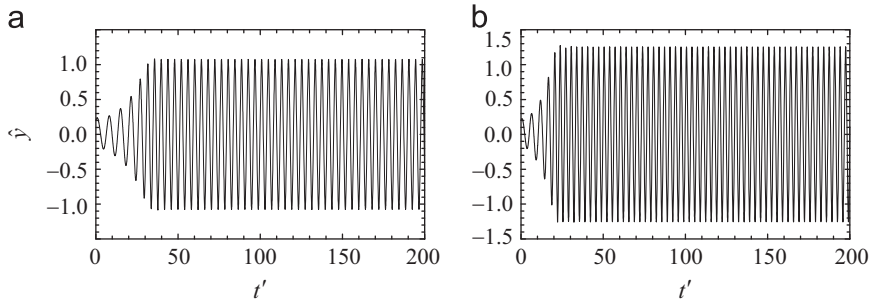

Fig. 12. The time-series response when the value of control strength and time delay are fixed in region 2 in Fig. 9 as (a) $g=0.3$, $\tau=4$; (b) $g=0.6$, $\tau=3$.

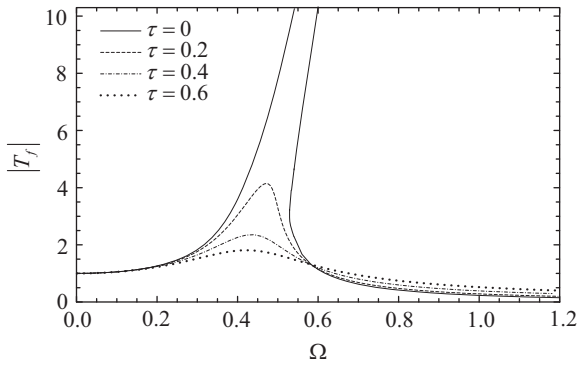

Fig. 13. The force transmissibility of the system under different time-delay as $\hat{f}=0.01$.

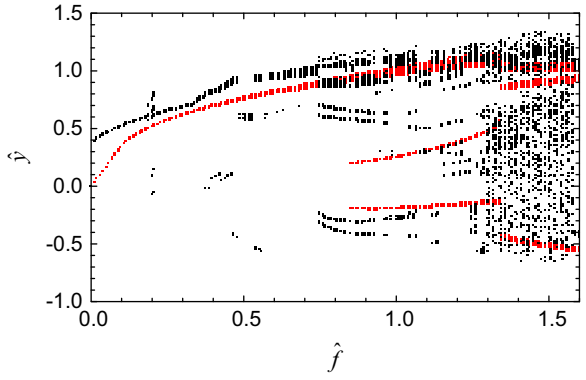

Fig. 14. The bifurcation diagrams with respect to the excitation amplitude. Black points are the motion without time-delay while red points are the motion at $g=0.5$, $\tau=1$. (For interpretation of the references to color in this figure legend, the reader is referred to the web version of this article.)

It should be noted that the jump phenomena are incurred by the inherent nonlinearity of the QZS-VI system, the excitation input can induce period-doubling bifurcation. With the amplitude of the excitation $\hat{f}$ increasing, the dynamics of the system become more complex. The instability of the secondary resonance and the separation of complex motion behaviors with different periods both potentially make a contribution to the occurrence of chaotic behaviors. The chaotic behavior in isolation of force sources is usually undesirable in practice, because the irregular dynamical behaviors may produce unpredictable damage to both the isolated equipments and the base as well as bring unpleasant noise. To explore the beneficial performance of the time delay in chaotic suppression, the effect of time-delayed active control on suppression of complex motion behavior can be studied using numerical simulations. The bifurcation diagrams of the response with respect to the amplitude of the excitation for $\tau=0$ and $\tau=1$ are shown in Fig. 14.

The black points in Fig. 14 are the response amplitude for $\tau=0$ while the red points are for $\tau=1$. The dynamic behavior of the system undergoes a series period-doubled bifurcation to chaos with the increase of $\hat{f}$ for $\tau=0$. However, for $\tau=1$, the period-doubled bifurcation just occurs when $\hat{f}$ reaches 0.7. From the bifurcation diagrams, it also can be seen that with the increase of the value of $\hat{f}$, the response of the system for $\tau=1$ has less frequency components in the motion than that for $\tau=0$. These clearly indicate that the time delay can play an important role in eliminate or suppress undesirable complex motion behaviors such as chaos in the isolation system.

3.3. Displacement transmissibility subject to base excitations

The case of base excitations simulates working conditions such as driving vehicles or ships. The vertical excitation from the base is $z_e(t)=z\cos(\omega_e t+\theta)$, the displacement of the isolated equipment relative to the base is y and the absolute displacement of the isolated equipment is z_a. The relative displacement and velocity of the isolated equipment satisfy the following relationships

$$y=z_a-z_e,\quad \dot{y}=\dot{z}_a-\dot{z}_e \tag{27}$$

Considering the time-delayed active control, the dynamical equation of the isolated equipment is as follows

$$M\ddot{y}+c\dot{y}+F(y)=k_3(y_\tau-y)-M\ddot{z}_e \tag{28}$$

The excitation of the base is $z_e=z\cos(\omega_e t+\theta)$ and the single mode response of the system is $y=A\cos\omega_e t$. The restoring force term $F(y)$ has been given in Eq. (2). After dimensionless transformation,

$$\tilde{y}=\frac{y}{z},\quad \hat{\lambda}=\frac{\lambda_0}{a},\quad \omega_0^2=\sqrt{\frac{k_0}{M}},\quad t'=\omega_0 t,\quad \tilde{F}(\tilde{y})=\frac{F(y)}{zk_0},$$
$$\alpha_1=\frac{k_1}{k_0},\quad \alpha_2=\frac{k_2}{k_0},\ g=\frac{k_3}{k_0},\quad \tau=\omega_0\tau',\quad \xi=\frac{c}{2\sqrt{Mk_0}},\quad \omega_e=\omega_0\Omega. \tag{29}$$

The dimensionless dynamical equation of the isolator system is

$$\ddot{\tilde{y}}+2\xi\dot{\tilde{y}}+\beta\tilde{y}+\tilde{\gamma}_1\tilde{y}^3+\tilde{\gamma}_2\tilde{y}^5=g(\tilde{y}_\tau-\tilde{y})-\Omega^2\cos(\Omega t'+\theta) \tag{30}$$

where $\tilde{\gamma}_1=(z^2/a^2)\gamma_1$, $\tilde{\gamma}_2=(z^4/a^4)\gamma_2$. Similar to the analysis in Section 3.2, the amplitude of the system under the base excitation can be described by a single-mode HBM solution as

$$\tilde{y}=\tilde{A}\cos(\Omega t') \tag{31}$$

where $\tilde{A}$ is the dimensionless amplitude of the response. Substituting Eq. (31) into Eq. (30) and neglecting the high harmonic terms, it can be obtained that

$$\left(\tilde{A}\beta+\frac{3}{4}\tilde{A}^3\tilde{\gamma}_1+\frac{5}{8}\tilde{A}^5\tilde{\gamma}_2-\tilde{A}\Omega^2\right)\cos\Omega t'-2\tilde{A}\xi\Omega\sin\Omega t'$$
$$=\Omega^2(\cos\theta\cos\Omega t'-\sin\theta\sin\Omega t')+\tilde{A}g(\cos\Omega\tau\cos\Omega t'$$

$$+ \sin \Omega\tau \sin \Omega t' - g \cos \Omega t') \tag{32}$$

Solving the coefficients of the same cosines and sines from Eq. (32), the steady state of the system satisfies the condition as

$$\begin{cases} \tilde{A}\beta - \tilde{A}\Omega^2 + \frac{3}{4}\tilde{A}^3\tilde{\gamma}_1 + \frac{5}{8}\tilde{A}^5\tilde{\gamma}_2 + \tilde{A}g - \tilde{A}g \cos \Omega\tau = \Omega^2 \cos \theta \\ 2\xi\tilde{A}\Omega + \tilde{A}g \sin \Omega\tau = \Omega^2 \sin \theta \end{cases} \tag{33}$$

Using $\sin^2\theta + \cos^2\theta = 1$, the frequency-amplitude curve is given as

$$\left(\tilde{A}\beta - \tilde{A}\Omega^2 + \frac{3}{4}\tilde{A}^3\tilde{\gamma}_1 + \frac{5}{8}\tilde{A}^5\tilde{\gamma}_2 + \tilde{A}g - \tilde{A}g \cos \Omega\tau\right)^2 + (2\xi\tilde{A}\Omega + \tilde{A}g \sin \Omega\tau)^2 = \Omega^4 \tag{34}$$

The vibration transmissibility T_d is defined as the ratio of the absolute displacement of the isolated equipment and the displacement of the base

$$T_d = \left|\frac{z_a}{z}\right| = \frac{\sqrt{A^2 + z^2 + 2zA \cos \theta}}{z} = \sqrt{\tilde{A} + 1 + (2\tilde{A}/\Omega^2)\left(\tilde{A}\beta - \tilde{A}\Omega^2 + \frac{3}{4}\tilde{A}^3\tilde{\gamma}_1 + \frac{5}{8}\tilde{A}^5\tilde{\gamma}_2 + \tilde{A}g - \tilde{A}g \cos \Omega\tau\right)} \tag{35}$$

When the parameters of the system and the active control are fixed, the transmissibility characteristics of the isolator can be obtained. The vibration transmissibility of the system under a certain excitation frequency shows the effect of the active control in vibration isolation. If choosing $\hat{\lambda} = 0.2$, $a = 0.4$, the other parameters of the system can be determined by Eq. (29) which are $\hat{\lambda} = 0.2$, $a = 0.4$, $\beta = 0.1872$, $\tilde{\gamma}_1 = 10.56z^2$, $\tilde{\gamma}_2 = 40.125z^4$ and $z = 0.01$. Fig. 15 is the displacement transmissibility with respect to different values of the time delay for $g = 0.3$. The decrease of the displacement transmissibility at around the resonant frequency shows clearly the nonlinear effect of the time delay in vibration isolation. The peak value for $\tau = 0.6$ is much less than that without time delay. Also, the nonlinear jump phenomenon for $\tau = 0$ is completely eliminated with the increasing of the time delay.

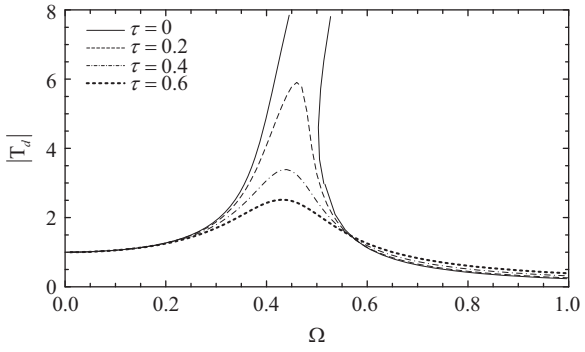

Fig. 15. The vibration transmissibility of the system under different time-delay as $g = 0.3$.

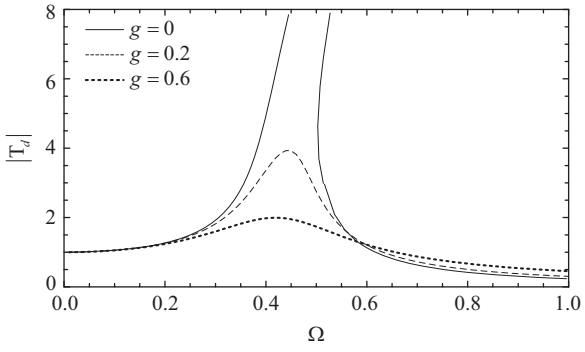

Fig. 16. The vibration transmissibility under different coefficient g as $\tau = 0.5$.

Fig. 16 shows the effect of the control strength g on the vibration isolation. For a fixed time delay $\tau = 0.5$, with the increase of control strength g, the vibration transmissibility at around the resonant frequency also decreases obviously.

From all the transmissibility results in Figs. 13, 15 and 16, it can be concluded that (a) the resonant frequency of the QZS-VI is very low (much less than 1), (b) the resonance peak can be significantly suppressed with properly-designed time delay in the active controller, (c) undesirable complex nonlinear behaviors such as chaos can also be effectively eliminated or suppressed using the time delay.

4. Conclusions

This paper provides a time-delayed active control strategy to improve the performance of a quasi-zero-stiffness vibration isolator (QZS-VI). The controlled spring and the time delay are used to form the active control structure. The important results provide a useful insight into both theoretical analysis and engineering design of nonlinear vibration isolators for superior vibration control performance and the results are represented as follows

1) The established delayed controller does not change the static features such as the equilibrium states but it may change the dynamical stability of the equilibria. The delay may be considered as a "switch" or an active control such that the delay or active control is easy to apply for the real engineering.
2) The controlled spring may efficiently change the nature frequency of the isolator so that the robustness in the dynamic stability for the equilibrium states is enhanced to achieve the control goal.
3) For the external impact load, an appropriate choice of the active delay may make the isolator accelerate the transient response so that the time history of the transient state is greatly shortened.
4) For the external harmonic load, it is found that the time delay has significant effect on vibration suppression for the resonant region. Thus, the delayed active control may extend the work range of the isolator without any structural modification. It means that one does not switch the delayed control for the effective working frequencies of the isolator but switch it when the isolator is invalid.

Acknowledgments

The authors, Xiuting Sun and Jian Xu would like to gratefully acknowledge the support from the State Key Program of National Natural Science Foundation of China under Grant no. 11032009, the Fundamental Research Funds for the Central Universities and Shanghai Leading Academic Discipline Project in No. B302 for this work; and Xiuting Sun, Xingjian Jing and Li Cheng would also like to gratefully acknowledge the support from the GRF project (Ref. 517810) of Hong Kong RGC, and internal Research Grants of Hong Kong Polytechnic University.

References

[1] Paddan GS, Griffin MJ. Evaluation of whole-body vibration in vehicle. J Sound Vib 2002;253:195–213.
[2] Jiang X, McFarland M, Bergman LA, Vakakis AF. Steady state passive nonlinear energy pumping in coupled oscillators: theoretical and experimental results. Nonlinear Dyn 2003;33:7–102.

[3] Kovacic I, Brennan MJ, Lineton B. Effect of a static force on the dynamic behaviour of a harmonically excited quasi-zero stiffness system. J Sound Vib 2009;325:870–83.
[4] Kovacic I, Brennan MJ, Waters TP. A study of a nonlinear vibration isolator with a quasi-zero stiffness characteristic. J Sound Vib 2008;315:700–11.
[5] Carrella A, Brennan MJ, Kovacic I, Waters TP. On the force transmissibility of a vibration isolator with quasi-zero-stiffness. J Sound Vib 2009;322:707–17.
[6] Ahn HJ. Performance limit of a passive vertical isolator using a negative stiffness mechanism. J Mech Sci Technol 2008;22:2357–64.
[7] Le TD, Ahn KK. A vibration isolation system in low frequency excitation region using negative stiffness structure for vehicle seat. J Sound Vib 2011;330:6311–35.
[8] Xing JT, Xiong YP, Price WG. Passive-active vibration isolation systems to produce zero or infinite dynamic modulus: theoretical and conceptual design strategies. J Sound Vib 2005;286:615–36.
[9] Carrella A, Brennan MJ, Waters TP, Lopes Jr V. Force and displacement transmissibility of a nonlinear isolator with high-static-low-dynamic-stiffness. Int J Mech Sci 2012;55:22–9.
[10] Cao QJ, Wiercigroch M, Pavlovskaia EE, Grebogi C, Thompson JT. The limit case response of the archetypal oscillator for smooth and discontinuous dynamics. Int J Non-linear Mech 2008;43:462–73.
[11] Tian RL, Cao QJ, Yang SP. The codimension-two bifurcation for the recent proposed SD oscillator. Nonlinear Dyn 2010;59:19–27.
[12] Cao QJ, Wiercigroch M, Pavlovskaia EE, Grebogi C, Thompson JT. Archetypal oscillator for smooth and discontinuous dynamics. Phys Rev E 2006;74:046218.
[13] Kovacic I, Brennan MJ, Lineton B. On the resonance response of an asymmetric Duffing oscillator. Int J Non-linear Mech 2008;43:858–67.
[14] Brennan MJ, Kovacic I, Carrella A, Waters TP. On the jump-up and jump-down frequencies of the Duffing oscillator. J Sound Vib 2008;318:1250–61.
[15] Huang SJ, Huang KS, Chiou KC. Development and application of a novel radial basis function sliding mode controller. Mechatronics 2003;13:313–29.
[16] Zhao YY, Xu J. Effects of delayed feedback control on nonlinear vibration absorber system. J Sound Vib 2007;308:212–30.
[17] Nana Nbendjo BR, Salissou Y, Woafo P. Active control with delay of catastrophic motion and horseshoe chaos in a single-well Duffing oscillator. Chaos, Solitons Fractals 2005;23:809–16.
[18] Nana Nbendjo BR, Tchoukuegno R, Woafo P. Active control with delay of vibration and chaos in a double-well Duffing oscillator. Chaos, Solitons Fractals 2003;18:345–53.
[19] Hackj K, Yang CY, Cheng AHD. Stability, bifurcation and chaos of non-linear structure with control-I. Autonomous case. Int J Non-linear Mech 1993;28:441–54.
[20] Raghothama A, Narayanan S. Bifurcation and chaos in geared rotor bearing system by incremental harmonic balance method. J Sound Vib 1999;226:468–92.
[21] Xu L, Lu MW, Cao Q. Nonlinear vibrations of dynamical systems with a general form of piecewise-linear viscous damping by incremental harmonic balance method. Phys Lett A 2002;301:65–73.